A Numerical Investigation of Blast Loading and Clearing on Small Targets

by

Sam E. Rigby, Andrew Tyas, Terry Bennett, Stephen D. Fay, Sam D. Clarke, James A. Warren

Reprinted from
International Journal of
Protective Structures

Volume 5 · Number 3 · September 2014

Multi-Science Publishing
ISSN 2041-4196

A Numerical Investigation of Blast Loading and Clearing on Small Targets

Sam E. Rigby[1*], Andrew Tyas[1,2], Terry Bennett[3], Stephen D. Fay[1,2], Sam D. Clarke[1], James A. Warren[1,2]
[1]Department of Civil & Structural Engineering, University of Sheffield, Mappin Street, Sheffield, S1 3JD, UK.
[2]Blastech Ltd., The BioIncubator, 40 Leavygreave Road, Sheffield, S3 7RD, UK.
[3]School of Civil, Environmental & Mining Engineering, North N136, North Terrace Campus, The University of Adelaide, SA 5005, Australia

Received on 17 Jan 2014, Accepted on 7 Apr 2014

ABSTRACT
When a blast wave strikes a finite target, diffraction of the blast wave around the free edge causes a rarefaction clearing wave to propagate along the loaded face and relieve the pressure acting at any point it passes over. For small targets, the time taken for this clearing wave to traverse the loaded face will be small in relation to the duration of loading. Previous studies have not shown what happens in the late-time stages of clearing relief, nor the mechanism by which the cleared reflected pressure decays to approach the incident pressure. Current design guidance assumes a series of interacting clearing waves propagate over the target face – this assumption is tested in this article by using numerical analysis to evaluate the blast pressure acting on small targets subjected to blast loads. It is shown that repeat propagations of the rarefaction waves do not occur and new model is proposed, based on an over-expanded region of air in front of the loaded face of the target.

Keywords: Blast, Clearing, Diffraction, Experimental Validation, Hudson, LS-DYNA, UFC-3-340-02

1. INTRODUCTION

When a mass of explosive material detonates it is converted into an extremely dense, high pressure gas. This reacting medium rapidly expands and displaces the surrounding air away from the source of the explosion at supersonic speed (faster than the speed of sound in the undisturbed air). The nature of air as a compressible fluid causes the pressure disturbance to form a shock front, a near discontinuous increase in pressure and density travelling outwards from the centre of the explosion [1].

When a blast wave reflects off a rigid target, conservation of mass, momentum and energy at the interface cause the pressure, density and temperature of the blast wave to be increased.

*Corresponding author. Tel.: + 44 (0) 114 222 5724. *Email address*: sam.rigby@sheffield.ac.uk

The magnitude of the pressures and impulses associated with the reflected blast wave are typically between 2 and 20 times greater than those of the free-air blast wave (known as 'incident' or 'side-on' values).

At the free edge of a target with finite lateral dimensions, whilst the reflected shock front begins to reflect away from the target surface, the incident shock front continues unimpeded past the edge of the target, causing diffraction around the free edge. At the same time, a pressure imbalance between the lower pressure incident wave and higher pressure reflected wave initiates flow between the higher and lower pressure regions and the pressure begins to equalise. The diffraction generates a low pressure rarefaction wave, which is driven by the flow conditions and travels along the loaded face, beginning at the boundaries and propagating in towards the centre of the target. As it passes over a point of interest, the rarefaction wave reduces the pressure acting on the loaded face, and hence reduces the total positive phase impulse imparted to the target.

The effect of blast wave clearing on the dynamic displacement of deformable finite targets has already been evaluated by the current authors [2–4], however the mechanism of blast wave clearing has not yet been fully explored, particularly for targets whose lateral dimensions are small in relation to the length of the blast wave.

This paper focusses on using numerical analysis to study blast wave clearing and diffraction loading on small targets in an attempt to better understand how the cleared reflected pressure decays to approach the incident pressure, and to evaluate the ability of approximate predictive methods to account for this behaviour.

2. LITERATURE REVIEW

The loading experienced by a point on a finite target remote from a free edge can be characterised by three distinct phases: firstly, the full reflected pressure will be experienced until the rarefaction clearing wave arrives; secondly, the blast pressure will be relieved as the expansion waves reach and propagate over the point of interest in what is termed the diffraction phase; thirdly, the drag phase occurs, where the diffraction process has ceased, the pressures have equalised across the front face of the target, and the target is subjected to quasi-steady drag loading [5].

The earliest observations of blast wave clearing appear to have been drawn from large scale nuclear bomb trials undertaken in the 1950s. Murtha [6] and Morris [7] report the findings from blast-pressure measurements taken from pressure transducers embedded within a 6 × 6 × 12 ft (1.8 × 1.8 × 3.6 m) structure situated 2200 ft (670 m) from the source ('ground-zero') of a nuclear blast. With such a small reflecting surface in relation to the length of the blast wave, the diffraction phase was short in relation to the positive phase duration, and any clearing effects were seen to dissipate very quickly and occurred relatively uniformly across the entire reflecting surface.

Accordingly, the early empirical clearing corrections – first introduced by Norris [8] and repeated in similar methodologies throughout the literature, including the Unified Facilities Criteria Design Manual UFC-3-340-02, *Structures to Resist the Effects of Accidental Explosions* [9] – only attempt to correct the entire impulse acting on the target, not the temporal or spatial distribution of cleared pressures. These empirical methods assume that clearing relief acts uniformly over the whole loaded face, beginning immediately at the time of arrival of the blast wave, and that the cleared blast pressure decays linearly from the peak reflected pressure to the stagnation pressure (the sum of the incident and drag pressure), over a characteristic clearing time, t_c, as in Figure 1.

This predictive methodology is based on the assumption that the cleared blast pressure is reduced by an infinite series of interacting expansion waves, each with diminishing

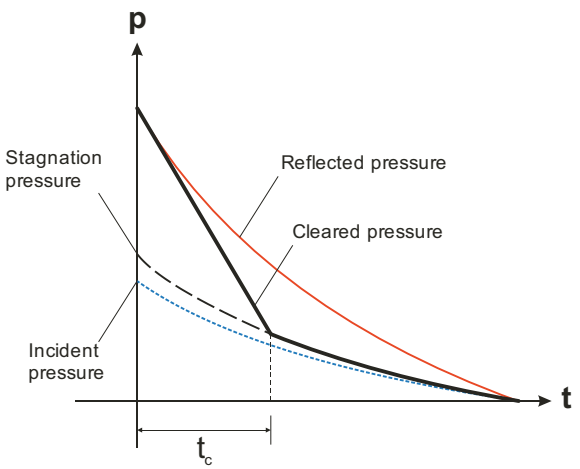

Figure 1. Clearing corrections from UFC-3-340-02 (9)

strength, travelling back and forth across the target face [10]. The net effect of this is, after a *given number of expansion wave crossings*, the cleared blast pressure effectively reaches the stagnation value and subsequent expansion wave crossings can be neglected. As noted by Hudson [11] *'we should expect oscillations of rather large amplitude… these oscillations are caused by the movement of the rarefaction and compression waves around the target'*.

This behaviour can be illustrated in a shock front distance-time diagram, as per Figure 2, which schematically shows clearing wave oscillations across the front of a finite-sized target. The main plot of Figure 2 shows the location of the shock front along the vertical front face of the target and the sub plots show the location of the shock fronts in relation to the target at times t_i, t_{ii} and t_{iii}, as indicated by the vertical dashed lines in the main plot. It can be seen that once the initial diffraction wave reaches the base of the target (between t_i and t_{ii}) it is reflected upwards. Once this wave reaches the top edge of the target (between t_{ii} and t_{iii}), it too initiates a diffraction wave which itself travels along the front of the target, reflects off the base and diffracts again upon reaching the vertical edge of the target. This process is repeated in an infinite series with each wave having decreasing magnitude. Given a large enough number of expansion wave crossings (i.e. a small sized target in relation to the blast length) the blast pressure will oscillate about and eventually approach the stagnation pressure as a limit.

The sign convention of Figure 2 is that positive vertical particle accelerations are coloured red, whilst negative (downward) vertical particle accelerations are shown in blue. At this stage, it is important to distinguish between *particle* motion and *wave* motion: in the main plot, which shows the shock front location, the colour indicates the particle motion whereas the gradient of the line indicates the wave velocity. It can be seen in Figure 2(t_{ii}) that the reflected diffraction wave is accelerating the particles downwards whilst the wave front itself is propagating upwards (in the subplots of Figure 2, arrows on the shock fronts indicate direction of wave propagation). Expansion waves occur when the particle acceleration is in the opposite direction to wave propagation, and compression waves occur when the respective motions are in the same direction. This sign convention is used throughout this article.

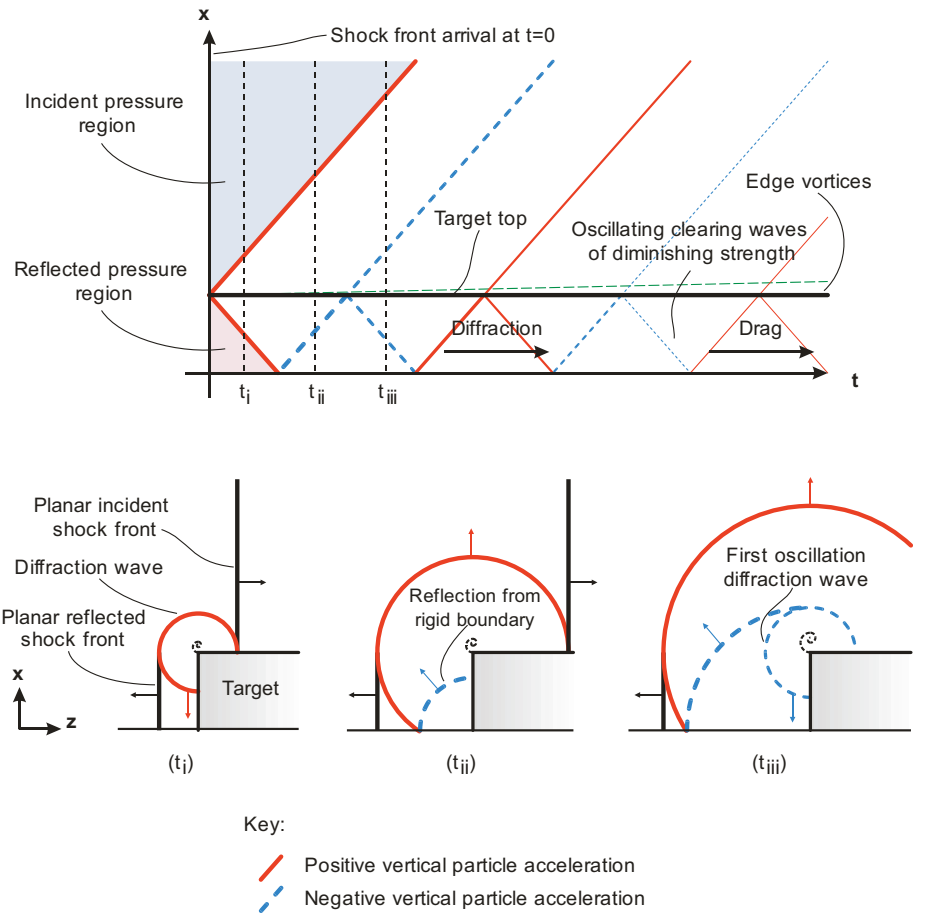

Figure 2. Schematic shock front distance-time diagram for a series of clearing waves travelling across the target face. Subplots show shock front progression at the times indicated

Rose & Smith [12] and Rickman & Murrell [13] developed improved empirical methodologies for predicting clearing relief, based on numerical analysis and experimental data respectively. Recently, Tyas et al. [14, 15] presented experimental validation of Hudson clearing corrections [11], based on the approximation of the relief wave as an acoustic pulse. These clearing corrections were shown to be able to predict the cleared blast pressure acting on larger targets whose loading is dominated by the diffraction phase and demonstrated excellent correlation with experimental results.

In his discussion of drag loading for small targets, Hudson [11] observed that *'as an approximation, we may write from our experience that the pulse associated with a wave having traveled* (sic) *more than the length of the originating edge is negligible'*, i.e. only one traverse of the expansion wave was seen to affect the recorded blast pressure. This suggests that blast wave clearing is not properly understood for smaller target dimensions and that the series of expansion wave interactions may be a misinterpretation of diffraction loading on small targets. Previous work has not shown how the Hudson predictions perform for smaller

targets, nor has previous work shown what the form of the blast pressure load is for targets whose dimensions are small enough such that the diffraction phase is resolved relatively early on during load application.

3. THE ALE METHOD

In this study, explicit finite element software LS-DYNA [16] is used to determine the blast pressure acting on rigid, finite-sized targets. The Arbitrary Lagrangian Eulerian (ALE) method is a scheme for solving the governing equations for conservation of mass, momentum and energy for compressible flow of a moving control volume flowing through a mesh, where the mesh moves with an arbitrary velocity relative to the material velocity.

In LS-DYNA, the ALE method is solved in two steps known as an operator split. First the governing equations are solved with the mesh velocity set as equal to the material velocity and a Lagrangian cycle is performed. After this, the deformed mesh is transported back to its original (un-deformed) position as mass, energy and momentum are transported across element boundaries in an Eulerian process, known as the advection phase. This process is shown schematically in Figure 3.

The ALE method is attractive for simulating blast events because excessive mesh deformations associated with Lagrangian formulations are avoided due to the advection 're-mapping' process. The ALE method is also more capable of handling multi-material formulations and tracking material interfaces than Eulerian formulations [17]. In this study, the Van Leer advection method with Half-Index shift [18] is used for the advection stage, as is recommended for high explosive problems [16].

3.1. MATERIAL MODELS AND EQUATIONS OF STATE

An Equation of State (EOS) expresses the relationship between the pressure, p, specific volume, V, and specific energy, E, of a fluid. In this study, is modelled as an ideal gas with MAT_NULL and EOS_LINEAR_POLYNOMIAL material model and EOS respectively. The linear polynomial equation of state is given as

$$p = C_0 + C_1\mu + C_2\mu^2 + C_3\mu^3 + (C_4 + C_5\mu + C_6\mu^2)E \tag{1}$$

where C_0, C_1, C_2, C_3, C_4, C_5, C_6 are constants and $\mu = \rho/\rho_0 - 1$. For ideal gasses, $C_0 = C_1 = C_2 = C_3 = C_6 = 0$ and $C_4 = C_5 = \gamma - 1$ and the equation reduces to the ideal gas equation of state

$$p = (\gamma - 1)\, E\rho/\rho_0 \tag{2}$$

Where ρ and ρ_0 are the current and initial densities of air, E is the specific internal energy and γ is the ratio of specific heats: $\gamma = 1.4$ for air. The specific internal energy, $E = 253.4$ kPa gives an atmospheric pressure of 101.36 kPa.

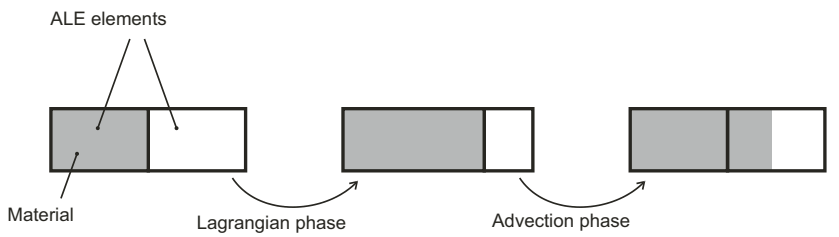

Figure 3. Lagrangian and Advection phases in an ALE analysis

Table 1. Material model and Equation of State parameters for air, TNT and C4 (SI units). Parameters for TNT and C4 are given in Dobratz & Crawford (22)

Air	MAT_NULL							
	ρ_0							
	1.225							
	EOS_LINEAR_POLYNOMIAL							
	C_0	C_1	C_2	C_3	C_4	C_5	C_6	E_0
	0.0	0.0	0.0	0.0	0.4	0.4	0.0	253.4E3
TNT	MAT_HIGH_EXPLOSIVE_BURN							
	ρ_0	D	PCJ					
	1630	6930	2.10E9					
	EOS_JWL							
	A	B	R_1	R_2	ω	E_0		
	371.2E9	3.231E9	4.15	0.95	0.30	7.0E9		
C4	MAT_HIGH_EXPLOSIVE_BURN							
	ρ_0	D	PCJ					
	1601	8193	2.80E10					
	EOS_JWL							
	A	B	R_1	R_2	ω	E_0		
	609.8E9	12.95E9	4.50	1.40	0.25	9.0E9		

If the detonation process is to be modelled – rather than applying empirical pressure predictions directly to the target [19] or to ambient air elements [20] – then a material model and EOS must be specified for the explosive. In LS-DYNA, MAT_HIGH_EXPLOSIVE_BURN is typically used, which requires the density, ρ, detonation velocity, D, and Chapman-Jouguet pressure, PCJ, of the explosive to be defined. Typically, the EOS used for high explosives is the Jones-Wilkins-Lee (JWL) empirical formula [21], EOS_JWL, which describes the pressure, volume, energy relation of the explosive as

$$p = A\left(1-\frac{\omega}{R_1V}\right)e^{-R_1V} + B\left(1-\frac{\omega}{R_2V}\right)e^{-R_2V} + \frac{\omega E}{V} \tag{3}$$

where A, B, R_1, R_2 and ω are constants, V is the volume and E is the internal energy. The arameters for air, TNT and C4 are shown in Table 1, with the JWL parameters for TNT and C4 given by Dobratz & Crawford [22].

4. VALIDATION OF BLAST MODELLING IN LS-DYNA

4.1. MODEL SETUP AND PRELIMINARY MESH STUDY

It is important that the limitations and sensitivity of a numerical model are understood so that physical effects can be distinguished from numerical effects when interpreting results. As such, a preliminary mesh study was undertaken: firstly, two different meshing techniques were evaluated; secondly, the chosen meshing technique was tested for sensitivity effects.

When modelling spherical charges in 2D axi-symmetry, it is common to model the explosive as a separate part within a radially symmetric mesh, as in Figure 4(a). Alternatively, the explosive can be modelled within a rectangular grid mesh, as in Figure 4(b), using the keyword *INITIAL_VOLUME_FRACTION_GEOMETRY with CONTYP = 6 (spherical container requiring the radius and coordinates of the origin of the sphere as input values) to 'fill' a volume in the mesh with the properties of the explosive part.

In the preliminary mesh study, a hemispherical TNT charge with 0.05 m radius (0.8535 kg) – detonated on a rigid ground surface and propagating through free air – was simulated using 2D axi-symmetric elements with material properties for air and TNT as outlined in Table 1. Default bulk viscosity parameters of 1.5 and 0.06 were selected based on the findings of an initial bulk viscosity study and were selected to minimise the energy lost through numerical dispersion at larger scaled distances [16].

The ground surface was modelled with nodal displacements constrained against vertical translation. For the radial mesh, contact between the explosive and air was achieved using shared nodes along the boundary, as this is both reliable and economic [23, 24]. The radial mesh contained 100,000 air elements and 11,700 explosive elements and the grid mesh contained 250,000 elements in total over a 1 m air domain.

Figure 5 shows the overpressure-time histories for both mesh techniques at a distance of 0.7 m from the centre of the explosive. It is clear from Figure 5 that the radial mesh is significantly less dispersive than the grid mesh. With the radial mesh, the spherical expansion of the shock wave is mainly aligned with the elements, whereas for the grid mesh, material transport occurs diagonally through elements. This introduces a second order advection error in LS-DYNA [16], hence when modelling spherical shock expansion a radially symmetric mesh should be preferred over a regular grid mesh. The radial mesh is also more efficient, as smaller elements are only located in areas of higher pressure gradient (closer to the centre of the charge), which can give a higher mesh resolution for a given run time compared to the grid mesh, or can give a shorter run time for a given minimum element (or time-step) size.

A mesh sensitivity analysis was conducted on the radial meshing technique. It was found that increasing the number of circumferential elements independent of the number of elements along the radius of the domain had little effect on the fidelity of the simulations. A fixed aspect ratio of 0.2 was chosen for the air elements, which is greater than the value of 0.1 as suggested by Hallquist [16] for stability purposes, and will be no less accurate than a mesh comprising more circumferential elements. The mesh sensitivity study was thus focused on the number of elements along the radial length of the domain (i.e. in the direction

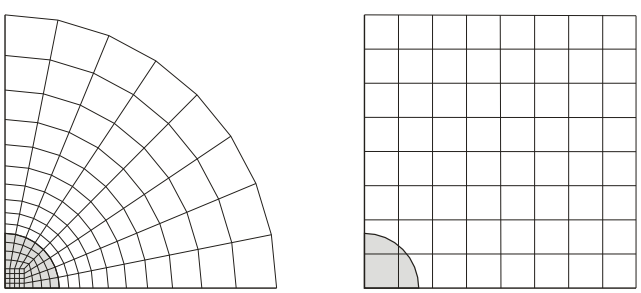

Figure 4. Representation of (a) radial mesh and (b) grid mesh used in the preliminary mesh study

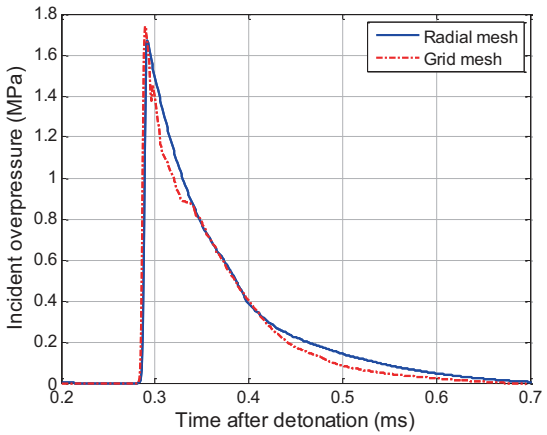

Figure 5. Overpressure-time histories for 0.8535 kg TNT spherical air burst at 0.7 m for radial and grid mesh

of the blast wave propagation), the results of which are presented here. A mesh sensitivity analysis was conducted for mesh densities ranging from 1,125 axi-symmetric elements (with 10 elements along the circumference and 100 elements along the radius of the air domain) to 446,800 axi-symmetric elements (with 200 elements along the circumference and 2000 elements along the radius of the air domain).

Incident pressure-time and impulse-time histories were evaluated for three gauge locations – 0.5, 0.7 and 0.9 m from the centre of the explosive. Figure 6 shows the pressure-time and impulse- time histories for the numerical analysis in free air at 0.7 m from the source of the explosive, for a fine mesh (comprising 446,800 elements), a medium mesh (27,975 elements, with 50 elements along the circumference and 500 elements along the radius of the air domain) and a coarse mesh (1,125 elements), all with an aspect ratio of ~0.2 for air elements. ConWep [25] positive phase pressure and impulse predictions, based on automation of the Kingery & Bulmash [26] empirical 'look-up' method, are also shown.

The influence of mesh density on resolution of the shock front can clearly be seen, with the discontinuity being smeared over ~25 μs for the coarsest mesh but being better represented by the finer meshes. Mesh density has less of an effect on the incident impulse,

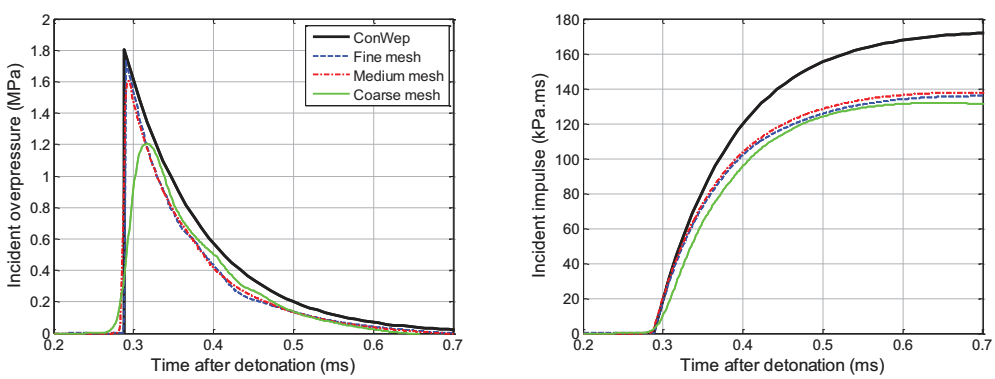

Figure 6. Incident pressure-time and impulse-time histories at 0.7 m from the explosive centre for fine, medium and coarse radial meshes

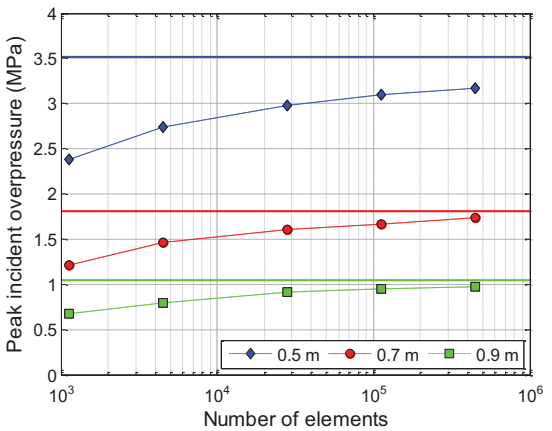

Figure 7. Peak incident overpressure for different mesh densities at three gauge locations. Solid lines indicate values given by ConWep (25)

suggesting that similar amounts of energy are released from the detonation process regardless of the mesh. Alia & Souli [24] suggest that no less than 16 elements are required along the radius of the explosive to accurately model the detonation process. For the coarsest mesh, 15 elements were used along the radius of the charge and similar amounts of energy were released when compared to the finer meshes, suggesting that this observation is valid.

Figure 7 shows peak incident overpressure for different mesh densities at all three gauge locations. The solid lines indicate values of peak incident pressure given by ConWep. The results generally tend towards the empirical predictions for peak incident overpressure with increasing mesh density.

Overall, there is a good level of agreement between the empirical and numerical results for peak pressure. The numerical model consistently under-predicts the incident impulse given by ConWep, however the preservation of peak pressure suggests that this is not due to cumulative energy losses in the numerical model. In a review of simplified predictive methods, Bogosian et al. [27] found that ConWep predictions for incident impulse were on average 15% higher than experimental test results. In the experimental work of Tabatabaei et al. [28], it was found that ConWep incident impulses were up to 40% higher than the measured free-field impulses, suggesting there is an inherent over-conservatism in ConWep incident impulse predictions.

4.2. REFLECTED PRESSURE ON A SEMI-INFINITE SURFACE

In this section, the reflected blast pressure measurements in Rigby et al. [29] are used to validate LS-DYNA blast simulations. 250 g hemispherical PE4 charges (nominally similar to C4) were detonated 4 m, 6 m, 8 m and 10 m away from and orthogonal to a semi-infinite rigid reflecting surface. The charges were detonated on a 50 mm thick steel plate, placed on a level, flat concrete ground slab, enabling the detonation to be considered as a hemispherical surface burst. Empirical predictions are also provided in this section, which were evaluated from UFC-3-340-02 [9] reflected positive and negative phase parameters assuming a TNT equivalence of 1.2 after Tyas et al. [14, 15]. The negative phase was constructed using the cubic approximation of Granström [30], after the validation work in Rigby et al. [29].

The detonation process and subsequent blast wave propagation was simulated using an axi-symmetric radial mesh after findings from the initial mesh study, with a charge radius of

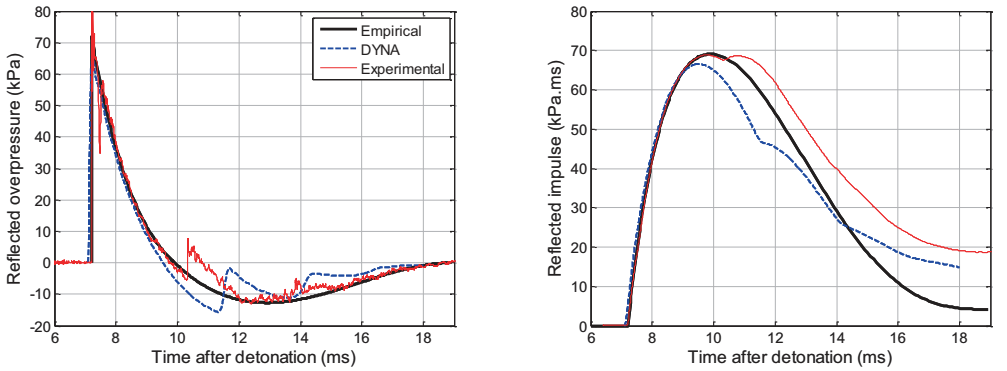

Figure 8. Reflected pressure-time and impulse-time histories for a semi-infinite rigid wall located 4 m away from a 250 g hemispherical PE4 charge

42.09 mm. One simulation was run with the blast wave propagating through free air, and separate map files were written at $t = 7.1$, 12.5, 18.0 and 23.8 ms after detonation, corresponding to travel distances of (less than) 4, 6, 8 and 10 m. The map files, which contained information of the incident wave, were re-mapped onto an axi-symmetric regular grid mesh to allow the planar structure to be modelled using only nodal constraints, with nodes along the boundary simulating the air/structure interface constrained against horizontal translations. The rigid ground surface was, again, modelled using vertical translational constraints. Performing the first stage of the analysis using the radial mesh and re-mapping onto a regular grid just before the blast wave strikes the target ensures that the blast wave arrives spherically symmetric whilst also simplifying the modelling of the reflecting surface. The explosive was modelled as C4, with JWL parameters taken from Dobratz & Crawford [22], shown in Table 1.

Figure 8 shows the pressure-time and impulse-time histories for the experiment, empirical prediction and numerical simulation at a stand-off of 4 m. Table 2 shows empirical and numerical values of peak reflected pressure, positive phase impulse and net impulse for all four stand-offs.

Overall, the numerical model is in very good agreement with both the empirical predictions and the experimental results for the positive phase of loading, although a small amount of numerical dispersion can be seen following the shock front. The numerical model is able to predict the peak pressure to within 9% of the empirical method. It is not applicable to show peak experimental pressures because of the large amount of sensor ringing in the experimental

Table 2. Pressure and impulse given by ConWep and DYNA for 0.25 kg hemispherical PE4 charge (0.3 kg TNT equivalence)

Stand-off (m)	Peak overpressure (kPa)			Positive impulse (kPa.ms)			Net impulse (kPa.ms)	
	Empirical	DYNA	Ratio	Exp.	DYNA	Ratio	Exp.	DYNA
4	71.9	67.7	0.94	68.8	66.7	0.97	18.4	17.5
6	37.1	33.9	0.91	44.8	40.0	0.89	6.6	7.1
8	24.5	24.5	1.00	32.6	29.7	0.91	1.9	–1.6
10	18.1	16.7	0.92	24.9	21.9	0.88	–2.8	–0.6

trials immediately after the shock wave arrival. The duration of the positive phase is shorter than observed in the experimental results, which leads to slightly reduced values of positive phase impulse in the numerical simulations. The form of the negative phase is well represented by the empirical predictions, which generally tend to follow the experimental measurements [29]. There are some differences between the negative phase parameters predicted by the numerical model and those from the experimental test data and empirical predictions. Typically, the numerical model predicts a slightly higher peak negative pressure and a slightly shorter duration of the negative phase. However, it can be seen in Table 2 that the positive phase (peak) impulses and total (net) impulses are generally in agreement between experiment and simulation for all stand-off distances. It is not useful to present ratios of numerical and experimental net impulse due to the proximity of the results to zero.

The physical process of the 'second shock' is captured in the numerical model, however the arrival time is over-predicted. The magnitude of this second shock is typically less than 10% of the main shock and, although it does affect the impulse transmitted through the shock, it is not of primary concern; the effects of clearing for small targets will cease long before the arrival of the second shock and hence the matter does not warrant further study here.

Peak pressures, peak impulses and net impulses associated with the experimental, numerical and empirical results are summarised in Figure 9. As the second shock arrives during the negative phase it acts to reduce the negative impulse and increase the net impulse acting on the target. Because the empirical method has no means to account for the second shock these predictions for net impulse appear to offer lower bound estimates, which become more accurate at larger stand- offs as the magnitude of the second shock decreases.

4.3. REFLECTED PRESSURE ON A FINITE SURFACE

With the detonation process, blast wave propagation and reflection already validated for the numerical model, the experimental results from Tyas et al. [14, 15] are used in this section to validate the ability of LS-DYNA to simulate the pressure acting on a finite target subjected to a cleared blast load, i.e. the ability of the model to capture clearing effects.

A rigid, 710 × 675 mm finite target, with gauges located along the vertical centerline of the target, as shown in Figure 10, was subjected to the blast pressure arising from the detonation of 250 g PE4 charges again at 4, 6, 8 and 10 m, with the presence of target edges able to influence the late-time pressure development on the face of the target. In this test

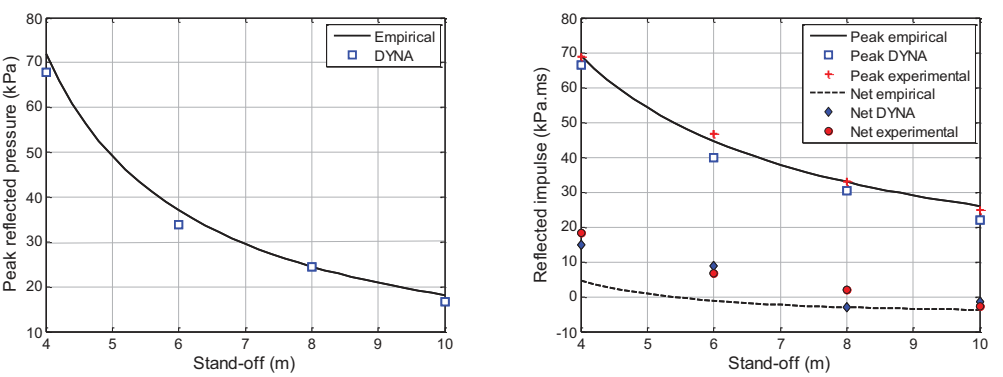

Figure 9. Peak pressure, positive phase (peak) impulse and total (net) impulse for the experimental results and numerical simulations compared to empirical predictions

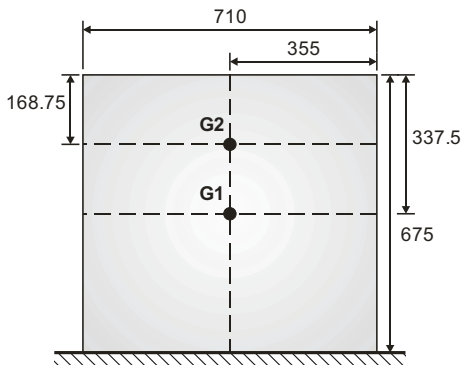

Figure 10. Gauge locations in the finite target (dimensions in mm)

series, two experiments were conducted at each stand-off. As with the semi-infinite target trials, the hemispherical charges were detonated on a rigid ground surface.

The mapping files written from the analyses in the previous section were re-mapped onto a 3D domain of solid ALE elements. When re-mapping from 2D to 3D, it is important to be aware of two conflicting issues:

Firstly, the 3D mesh must be large enough to contain a sufficient 'length' of the blast wave [31]. For the 10 m simulation, a positive phase duration of ~3.6 ms and an assumed wave speed of 340 m/s gives the positive phase wavelength as 1.2 m, i.e. the ALE domain must be at least this length in front of the target to capture the whole of the positive phase. If the entire negative phase is to be re-mapped, domain lengths of ~5 m are required. It is also important to have the domain large enough to ensure that expansion waves from the edge of the domain do not reach the monitoring points during the analysis and contaminate results [20].

Secondly, as demonstrated in the mesh sensitivity study, ALE analyses are very sensitive to mesh refinement, particularly when considering the resolution of the shock front. The elements in the ALE domain should therefore be small to ensure sufficient fidelity of the results, however it is often not possible to achieve similar mesh densities between 2D and 3D analyses. In this validation, it was important to examine the mechanism of clearing and the reduction of positive phase pressure, so a 1 m domain was chosen to allow analysis durations of ~3 ms. The domain was discretised using elements of side length 17.5 mm. As with the 2D case, the rigid target was modelled with nodal constraints rather than fluid-structure interaction. Half-symmetry was used, with appropriate boundary conditions along the vertical boundary. The rigid ground was again modelled with boundary conditions.

Figure 11 shows the numerical and experimental pressure-time histories for both gauge locations for the 4 m stand-off trials. A smoothing of the shock front can be seen as a result of mapping from a fine mesh to a coarser mesh, however the agreement between numerical and experimental results is very good, and the numerical model is able to capture the physical process of blast wave clearing to a sufficient level of accuracy.

Table 3 shows the peak impulse for the experiments and numerical simulations for all stand-offs and at each gauge location. The experimental values are taken as the average between the two tests. Overall, the numerical impulse is within 12.5% of the experimental results, with a general trend towards increasing difference with increasing stand-off, which is likely due to numerical dispersion. Table 3 is also summarised in Figure 12, which shows the un-cleared predicted impulses from ConWep as an indication of the level of impulse reduction attributed to blast wave clearing.

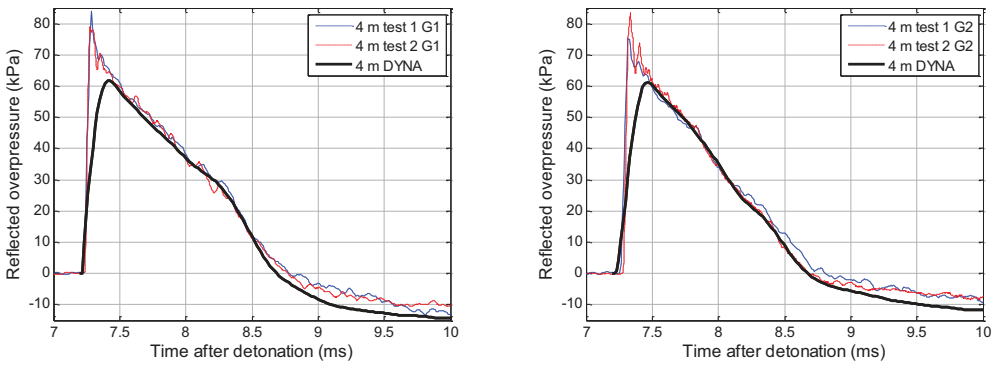

Figure 11. Experimental and numerical pressure-time histories for two gauge locations on a finite target located 4 m away from a 250 g hemispherical PE4 charge. Gauge locations and target dimensions are shown in Figure 10

Table 3. Peak reflected impulse comparison for numerical and experimental trials in both gauge locations, *denotes an averaged result between two experiments

Stand-off (m)	**Peak reflected impulse (kPa.ms)**					
	Gauge 1			**Gauge 2**		
	Exp.*	**DYNA**	**Ratio**	**Exp.***	**DYNA**	**Ratio**
4	56.5	52.0	0.92	50.8	46.9	0.92
6	32.6	30.2	0.93	29.3	27.3	0.93
8	22.8	20.9	0.92	20.9	19.2	0.92
10	17.4	15.2	0.87	16.2	14.2	0.88

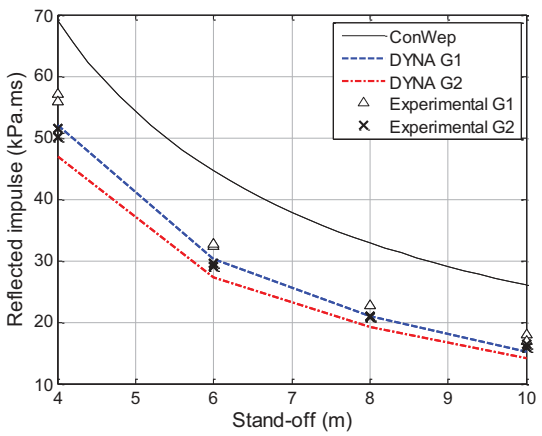

Figure 12. Numerical and experimental peak impulse at both gauge locations for all stand-offs. NB: ConWep data is for un-cleared impulse

5. NUMERICAL STUDY

With a well validated model, it is possible to use finite element analysis to study fundamental physical processes, such as the mechanism of clearing on targets whose diffraction phase constitutes a small part of the positive phase duration. It has been shown that clearing on the front face of 3D rectangular targets can be separated into two principal directions [14]. For 'step' targets, i.e. targets with effectively infinite vertical width and depth but with finite height, clearing will occur over the top edge only, and the problem can be represented in 2D. The 2D situation will also apply to structural columns, where the height of the column is very large in relation to the width and clearing can be assumed to occur over the side edges of the column only, with the centreline of the column acting as a symmetry boundary, nominally identical to a rigid reflecting surface. This justification permits the use of a finer mesh than would be possible if clearing were considered over the top *and* side edges of the target and the model were analysed in 3D.

For the numerical study, the situation in Figure 13 was considered, with a 1 kg TNT charge detonated 8 m away from rigid, finite-sized step targets (or columns), with target heights (or column half-widths) of 31.25, 62.5, 125 and 250 mm, corresponding to $S = Z/256$, $Z/128$, $Z/64$ and $Z/32$, where S is the target height and Z is the stand-off. The model was also run with free-field conditions and with an infinite sized target so that the cleared readings could be compared against the incident and fully reflected cases. The *DATABASE_TRACER keyword was used to save fixed point values (with the variable TRACK = 1) at 10 mm spacing from $x = 0$ (ground level) up to $x = 1$ m for all analyses. Detonation and free-air propagation was modelled in a radial domain and, once the blast wave had travelled 8 m, the information was re-mapped onto a rectangular mesh to model blast-target interaction.

5.1. PRESSURE-TIME HISTORY

Figure 14 shows numerical pressure-time histories at the base of the targets, $p_{x=0}$, as well as reflected pressures, p_r, and incident pressures, p_{so}, for reference. For a 1 kg hemispherical surface burst at 8 m stand-off, ConWep gives empirical peak reflected and incident pressures and positive phase duration as 44.11 kPa, 20.34 kPa and 4.454 ms respectively, which are in good agreement with the numerical values.

The effect of blast wave clearing is apparent from the pressure-time traces, which exhibit a sharp drop off in pressure following the arrival of the rarefaction relief wave. What is apparent, however, is that there appears to be no trace of any subsequent oscillations of the cleared pressure caused by additional diffraction waves, as the current

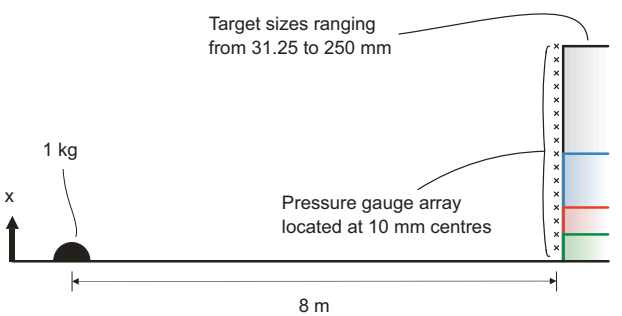

Figure 13. Arrangement of the FE models considered in the numerical study

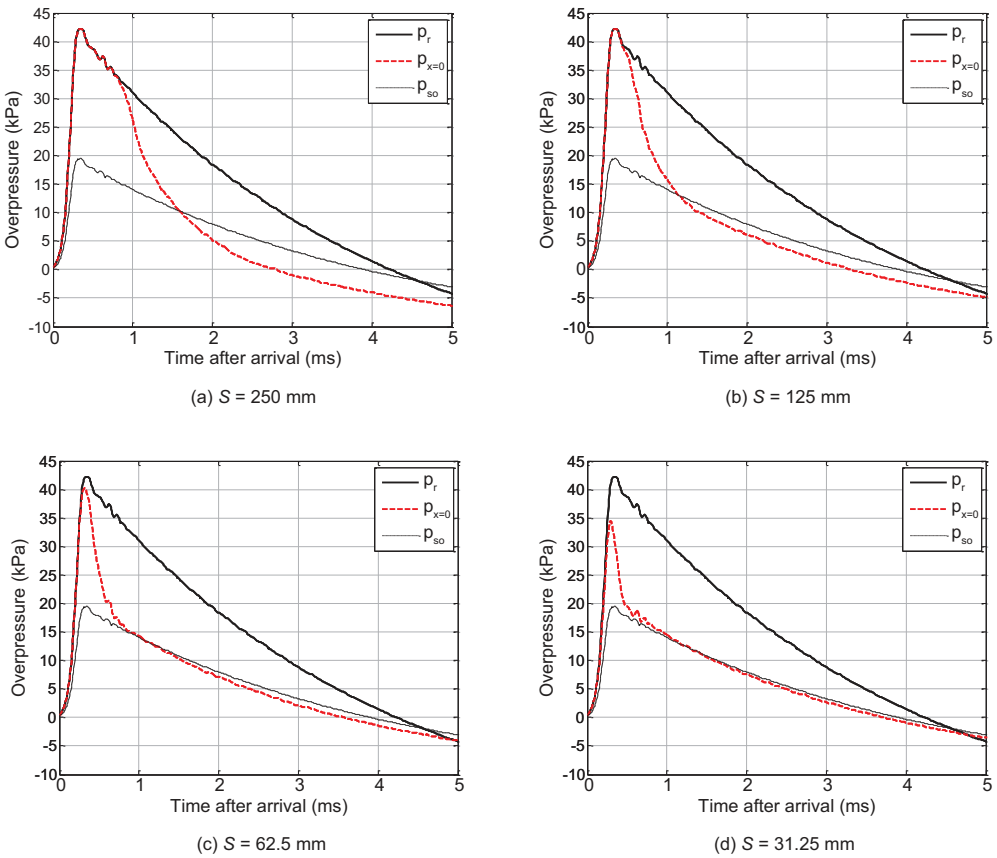

Figure 14. Pressure-time histories at the base of the finite targets (x = 0)

theory suggests there should be. Take Figure 14(a) as an example. With a target height, S, of 250 mm, the time taken for the clearing wave to reach the gauge location from the top of the target will be 0.74 ms after arrival of the blast wave (assuming a clearing shock front velocity of 340 m/s). This first wave is clearly seen in the numerical model. Assuming the clearing shock front velocity remains unchanged, one would expect to see a positive oscillation (pressure increase) at 2.21 ms, and a subsequent negative oscillation (pressure decrease) at 3.68 ms after the arrival of the blast wave. These times correspond to odd multiples of the traverse time of the clearing wave, i.e. the time taken to travel from the top of the target to the bottom for the first wave, and the additional time taken for the wave to travel from the bottom of the target to the top and back again for the first positive oscillation, etc.

It is acknowledged that the clearing wave should be expected to lose energy as it propagates, and that the diffracted signal will be lower in magnitude than the original clearing wave, however some oscillations should still be expected to be seen based on the current theory, particularly for the smaller targets where the energy losses from propagating the small distances across the target face will be negligible.

There are pressure oscillations apparent at around 0.6 ms for S = 31.25 mm which appear to follow the head of the clearing wave, however this is a numerical (non-physical) feature

which can be seen to be present in the reflected pressure traces for all of the numerical results and should not be interpreted as physical behaviour of the clearing shock front. The absence of non-numerical oscillations, therefore, is in agreement with the experimental observations of Hudson [11].

Following the passing of the expansion wave, the pressure acting on the target face falls below and remains below the incident pressure. The air remains over-expanded for the remainder of the loading duration rather than experiencing pressure oscillations. This suggests that the blast pressure does not approach the stagnation pressure but instead reaches and maintains a pressure somewhat below this value. It appears as though the over-expansion of the air is a function of target size, and that the larger the target the more the clearing wave causes the air in front of the target to over-expand. This behavior deviates from the current theory and deserves further consideration.

5.2. PARTICLE ACCELERATION-TIME HISTORY AND THE MECHANISM OF CLEARING

Figure 15 shows numerical vertical particle acceleration-time fringe plots for the finite-sized targets at the gauges located vertically along the target face and in the free air above (see Figure 13). The free field particle acceleration has been subtracted from the cleared

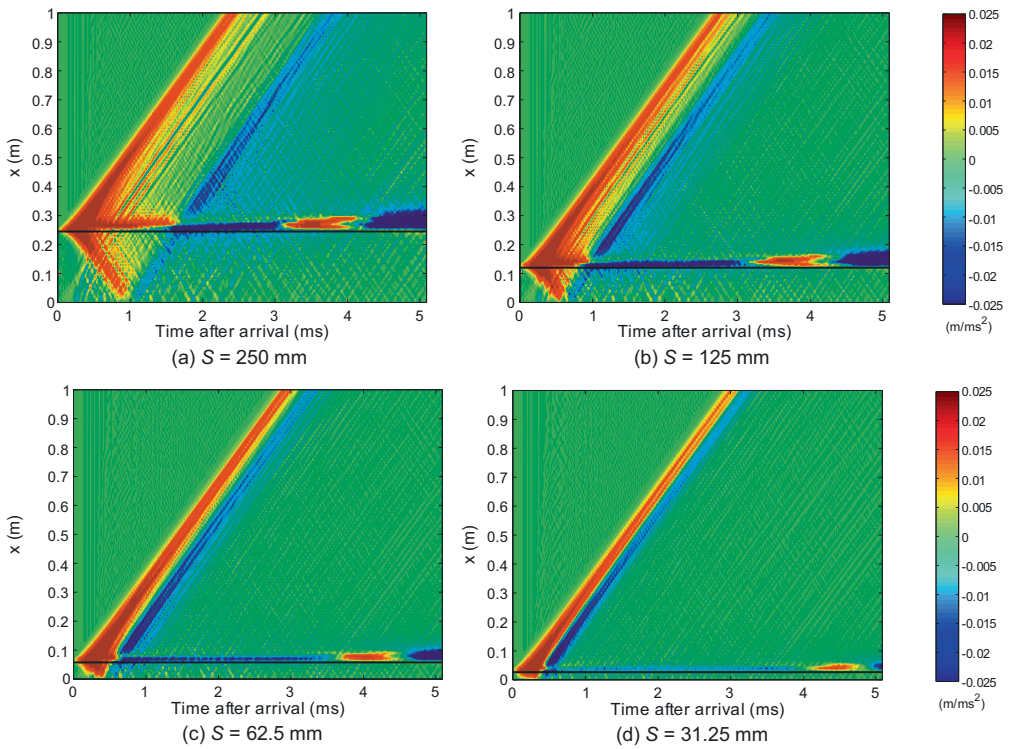

Figure 15. Fringe plots of cleared particle acceleration minus incident particle acceleration versus time for gauge locations aligned vertically along the front face of the target (arrangement shown in Figure 13). Target top edge (x location) is indicated by the solid horizontal line

particle acceleration to isolate and better present the effects of clearing. Acceleration-time plots are analogous to the slope of the pressure-time plots and can be used to construct shock front distance-time diagrams as per Figure 2. The gradient of any shock front will, to some extent, always be dependent on the length of the elements, hence the magnitude of the acceleration should be considered less important than the actual sign, or direction, of acceleration. Figure 15 follows the sign convention introduced earlier in this article, with red indicating positive vertical particle acceleration and blue indicating negative vertical particle acceleration.

When the blast wave reaches the top edge of the target, an expansion wave can be seen to travel downwards, beginning at the free edge, whilst a compression wave can be seen to travel upwards through the air immediately above the target, both waves orthogonal to the direction of travel of the blast wave itself. Following reflection from the rigid boundary, the expansion wave changes direction and propagates back along the face towards the target edge, and beyond into the free air. The shock front emanating from the top edge of the target can be seen very clearly, as can the reflection (and sign reversal) off the rigid boundary. Again there appears to be no diffraction wave oscillation after the initial clearing wave has passed the edge of the target. This is true for all target sizes and is also true for the entire duration of loading after the passing of the initial clearing wave.

Based on evidence from the numerical analyses, the mechanism of blast wave clearing for smaller targets can be interpreted as follows:

- Upon reaching the edge of a finite target, the blast wave diffracts around the edge, causing a clearing wave to travel inwards along the target face. The wave is travelling *away* from the target edge but accelerating the particles *towards* the edge, hence acting as an expansion wave and reducing the pressure acting on the target.
- If the target is situated on a rigid ground surface, the wave then reflects off the surface and propagates back towards the origin of the clearing wave, i.e. the top edge of the target. If the target is subjected to a free air burst and is located some distance from the ground, the problem can be expressed as a hemispherical surface burst with a rigid ground surface by introducing a symmetry plane along the centre of the target in the direction of travel of the blast wave, and hence the process is identical. Reflection causes both the shock front velocity and the particle acceleration to reverse.
- This reflected clearing wave continues to propagate beyond the target into the free air above, decreasing in magnitude as it expands both vertically and horizontally. No diffraction waves are sent back along the target.
- A region of over-expanded air is present in front of the target, which expands outwards. The air behind this expanding shock front is in local equilibrium.

The net velocity applied at any point on a finite target is given as the sum of the 'disturbed' velocity applied by the first passing of the clearing wave, and the 'corrective' velocity applied by the reflected clearing wave, which acts in the opposite direction.

Clearly, for smaller targets, the distance travelled away from the point of interest to the rigid boundary and back again decreases, hence the energy lost through spherical expansion of the shock front also decreases and the corrective velocity approaches the disturbed velocity. This explains how the cleared blast pressure can be seen to approach the incident pressure from below as the target height decreases, i.e. how the over-expansion decreases with decreasing target height. This also gives a basis for the 'overshoot' pressure seen in experimental [13–15, 32, 33] and numerical results [12, 34]. A revised shock-front distance-time diagram is shown in Figure 16.

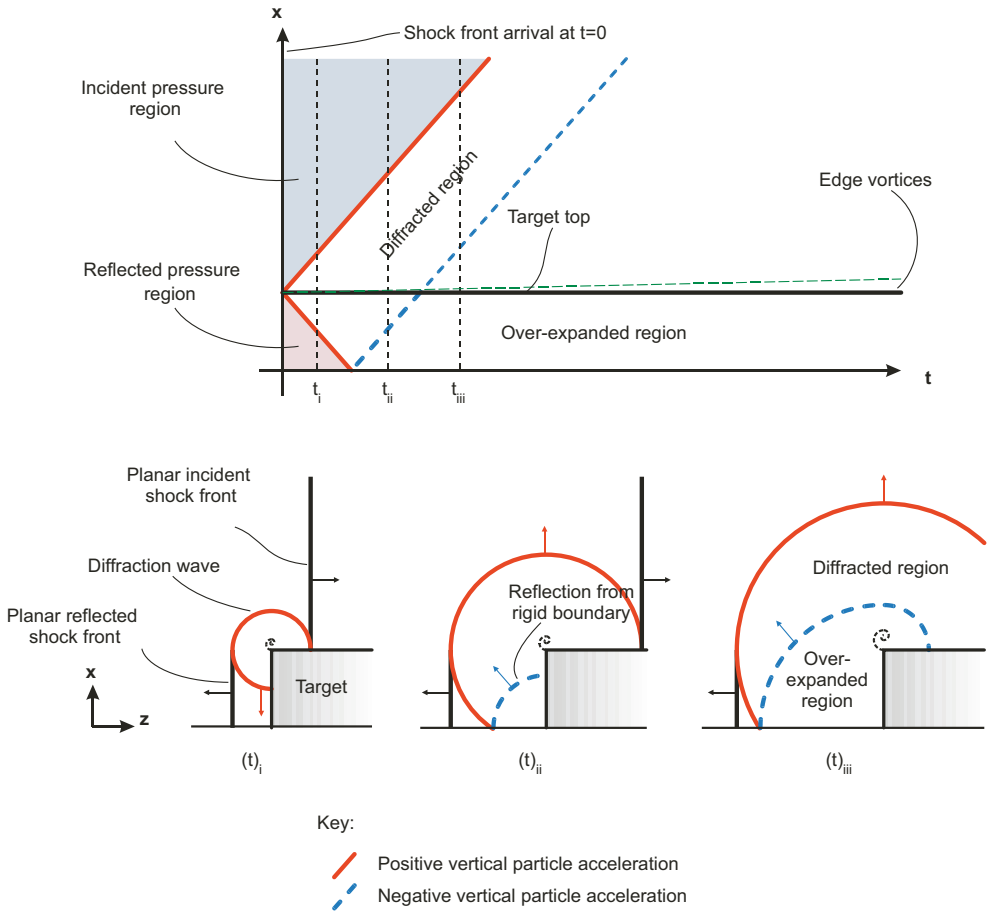

Figure 16. Schematic shock front distance-time diagram for a primary and secondary (reflected) clearing wave travelling across the target face and over-expanding the air in front of the target. Subplots show shock front progression at the times indicated

5.3. CLEARING PREDICTIONS

The empirical clearing methodology in UFC-3-340-02 [9] gives the clearing time, i.e. the time at which the diffraction phase has completed and all clearing effects have ceased, as

$$t_c = \frac{4S}{(1+R)a} \tag{4}$$

where

t_c = clearing time (s)
a = shock front velocity (m/s)
S = min[front height, half width] (m)
G = max[front height, half width] (m)
$R = S/G$ (-)

which gives $t_c = 0.73$, 1.09, 1.83 and 3.30 ms after arrival for the 31.25, 62.5, 125 and 250 mm targets respectively. S/a is the time taken for one expansion wave crossing and $R \approx 0$ for step

targets or columns, hence clearing is assumed to be completed after exactly 4 expansion wave crossings in this method. The pressure is assumed to decay linearly from peak reflected pressure to the stagnation pressure over the clearing time. As discussed previously, this method was developed from observations of cleared blast loading on targets subjected to large-scale nuclear blasts and hence should be suitable for the small relative target sizes considered in this study.

Tyas et al. [14, 15] experimentally validated the Hudson [11] method for predicting the cleared pressure acting on targets subjected to diffraction-type loading. In this validation, the time taken for the clearing wave to propagate across the target face was comparable to the duration of loading. One of the assumptions of the Hudson predictive method is that no flow conditions exist in the direction of travel of the clearing wave [11]. From the numerical study conducted in this article, it has been shown that the mechanism of clearing does not feature multiple rarefaction wave crossings but rather a single rarefaction wave originating from the free edge, propagating across the target face and into the incident air beyond the opposite edge of the target. It stands to reason, therefore, that the Hudson predictive method will still be able to predict the cleared pressure acting on small targets as there are no subsequent diffraction waves to consider aside from the original pulses.

Figure 17 shows the reflected, incident and cleared blast pressure at the base of the target from the numerical analyses (as in Figure 14). Also included are the UFC-3-340-02 [9] and

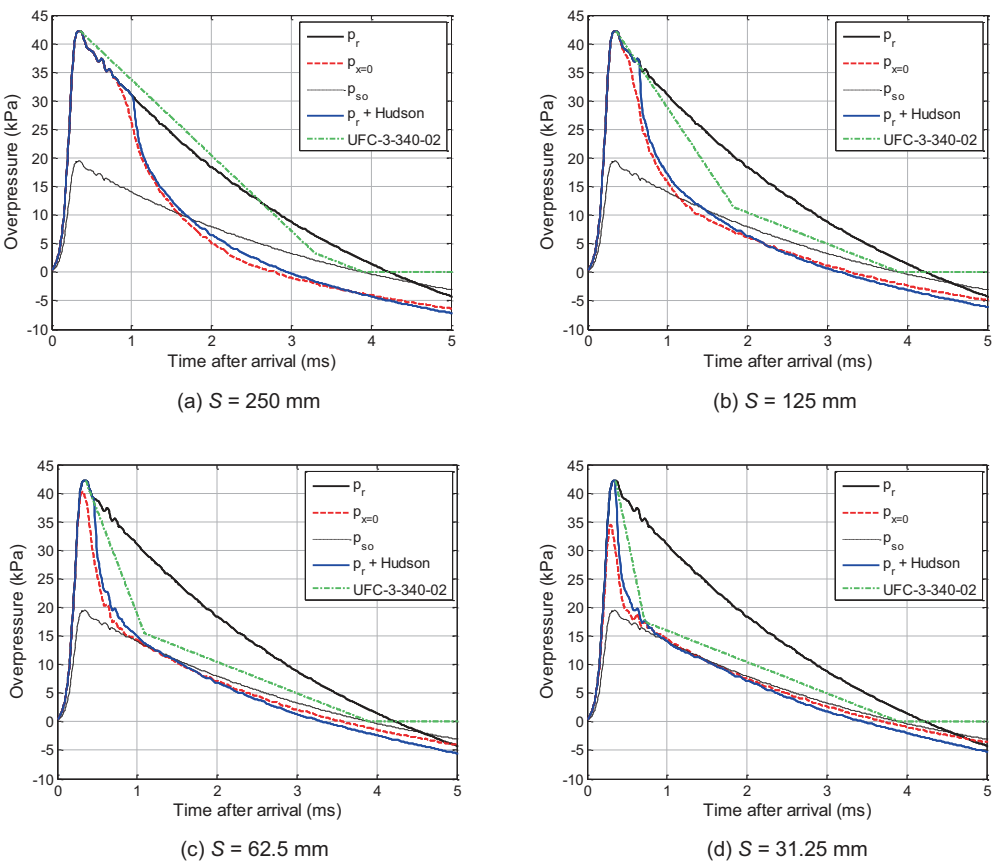

(a) S = 250 mm (b) S = 125 mm

(c) S = 62.5 mm (d) S = 31.25 mm

Figure 17. Pressure-time histories at the base of the finite targets (x = 0) with Hudson (11) and UFC-3-340-02 (9) clearing predictions

Hudson [11] cleared blast pressure predictions. The peak pressure was taken to occur at a time of 0.36 ms for the UFC-3-340-02 clearing predictions to account for numerical rounding of the shock front, and the incident pressure was assumed to decay linearly over the positive phase duration, from peak pressure at 0.36 ms to ambient pressure at 3.91 ms, corresponding to the time at which the incident numerical pressure reaches zero. No negative phase effects are accounted for in this method and the pressure remains at zero thereafter. The Hudson predictions are given as the superposition of the numerical reflected pressure and the cleared pressure relief functions given by the Hudson predictive method, the methodology of which is available in Refs. [3, 14].

The superposition of the numerical reflected pressure and the Hudson clearing corrections are in excellent agreement with the numerical cleared pressures for all the target sizes studied. This strongly suggests that given knowledge of the free-field and reflected blast load and geometry of the target, the cleared blast pressure can be accurately predicted using the Hudson method for any realistic target size.

Interestingly, the UFC-3-340-02 [9] empirical clearing predictions appear to be in better agreement for smaller target sizes. This is indicative of the fact that the original clearing corrections were based on observations from experimental cleared pressure measurements on targets whose lateral dimensions were in the order of metres, compared to stand-offs in the order of kilometres [6-8]. For these test configurations, the loading quickly approached the incident pressure relative to the positive phase duration – it can be seen that the UFC-3-340-02 clearing corrections are reasonably accurate until S exceeds $Z/250$, which should be taken as a limit for the use of this method. The fact that these predictions diverge from the cleared pressure for larger targets suggests that the method is unsuitable for situations where the diffraction phase constitutes a larger portion of the positive phase, whereas the Hudson clearing predictions have been shown to be valid for both drag-type and diffraction-type loading.

6. SUMMARY AND CONCLUSIONS

This paper has aimed to investigate the blast pressure load acting on finite targets where the presence of a free edge is known to cause a clearing wave to travel across the loaded face. For targets that are sufficiently small such that this clearing wave propagation constitutes a small portion of the loading duration, the process by which the incident pressure is reached and the typical form of the blast pressure load was previously unknown.

This process has been studied in this article through the use of numerical analysis. The Arbitrary Lagrangian Eulerian (ALE) method is introduced, and LS-DYNA is used to simulate explosive blast events. A mesh sensitivity analysis is conducted, where it was found that radially symmetric meshes should be used to model the detonation and spherical expansion of blast waves owing to a second order advection error introduced when modelling spherical blast wave propagation in non-spherical meshes. Experimental data has been used to validate reflected pressure modelling on semi-infinite and finite reflecting surfaces and it was found that LS-DYNA was capable of simulating such events to a good level of accuracy.

The validated computer model was then used to investigate the form of the cleared blast pressure load. Current literature guidance [9, 10] suggests that the mechanism of clearing is an infinite series of crossing diffraction waves, with each wave decreasing in magnitude, causing the blast pressure to oscillate about and, for small targets, rapidly approach the incident pressure.

It was observed that, rather than a series of crossing rarefaction waves, the cleared blast pressure features only one rarefaction wave from the free edge, which travels along the target

face, crosses with the clearing wave travelling from the opposite edge (for free air bursts), or reflects off the rigid ground surface (for surface bursts), and propagates past the target edge into the incident region beyond the extents of the target. This causes a region of over-expanded air (relative to the incident blast conditions) to exist in front of the target, with larger targets causing a greater over- expansion.

It has also been shown that, whilst the available methods for predicting clearing relief [9] appear suitable for predicting the blast pressure acting on small targets (or targets subjected to large blast events), they cannot be used to predict the pressure acting on larger sized targets or smaller blast events. Based on the numerical results from this article, it is suggested that if the target height for step targets – or the half-width for columns – exceeds $Z/250$, then the traditional methods for clearing predictions should not be used. It has already been shown that the Hudson [11] method can accurately capture the features of blast wave clearing for larger target sizes [14, 15], and it has been shown in this article that the method is able to also predict clearing for small target sizes, based on the fact that the load comprises only one clearing wave propagation across the target face from each free edge.

This article presents new observations on the mechanism of blast wave clearing, and provides evidence to question the validity of methods for predicting clearing that exist in the current literature.

ACKNOWLEDGEMENTS

The authors would like to express their gratitude to technical staff at Blastech Ltd. for their assistance in conducting the experimental work reported herein. The first author acknowledges the financial support from the Engineering and Physical Sciences Research Council (EPSRC) Doctoral Training Grant.

REFERENCES

[1] W. E. Baker. *Explosions in air.* University of Texas Press, Austin, TX, USA, 1973.

[2] S. E. Rigby, A. Tyas, and T. Bennett. Single-degree-of-freedom response of finite targets subjected to blast loading – the influence of clearing. *Engineering Structures,* 45:396–404, 2012.

[3] S. E. Rigby, A. Tyas, T. Bennett, J. A. Warren, and S. Fay. Clearing effects on plates subjected to blast loads. *Engineering and Computational Mechanics,* 166(3):140–148, 2013.

[4] S. E. Rigby, A. Tyas, and T. Bennett. Elastic-plastic response of plates subjected to cleared blast loads. *International Journal of Impact Engineering,* 66:37–47, 2014.

[5] N. H. Ethridge. *Blast diffraction loading on the front and rear surfaces of a rectangular parallelepiped*. ARBRL- MR-2784, U.S Army BRL, Aberdeen Proving Ground, MD, USA, 1977.

[6] J. P. Murtha. *Blast loading of structures in the regular reflection and low mach-stem regions*. SC-TM-5112, Sandia Corporation, MD, USA, 1955.

[7] W. E. Morris. *Shock diffraction in the vicinity of a structure*. Operation Upshot-Knothole, WT-786, Sandia Corporation, MD, USA, 1959.

[8] C.H. Norris, R. J. Hansen, J. H. Myle, J. M Biggs, S. Namyet, and J. K. Minami. *Structural Design for Dynamic Loads*. McGraw-Hill, New York, NY, USA, 1959.

[9] US Department of Defence. *Structures to resist the effects of accidental explosions*. US DoD, Washington DC, USA, UFC-3-340-02, 2008.

[10] W. J. Taylor. A method for predicting blast loads during the diffraction phase. *The Shock and Vibration Bulletin,* 42(4):135, 1972.

[11] C. C. Hudson. *Sound pulse approximations to blast loading (with comments on transient drag)*. SC-TM-191-55-51, Sandia Corporation, MD, USA, 1955.

[12] T. A. Rose and P. D. Smith. An approach to the problem of blast wave clearing on finite structures using empirical procedures based on numerical calculations. In *16th Symposium on the Military Aspects of Blast and Shock (MABS16),* pages 113–120. Oxford, UK, 2000.

[13] D. D. Rickman and D. W. Murrell. Development of an improved methodology for predicting airblast pressure relief on a directly loaded wall. *Journal of Pressure Vessel Technology,* 129(1):195–204, 2007.

[14] A. Tyas, J. Warren, T. Bennett, and S. Fay. Prediction of clearing effects in far-field blast loading of finite targets. *Shock Waves*, 21(2):111–119, 2011.

[15] A. Tyas, T. Bennett, J. A Warren, S. D. Fay, and S. E. Rigby. Clearing of blast waves on finite-sized targets – an overlooked approach. *Applied Mechanics and Materials*, 82:669–674, 2011.

[16] J. O. Hallquist. *LS-DYNA Theory Manual*. Livermore Software Technology Corporation, CA, USA, 2006.

[17] M. Souli, A. Ouahsine, and L. Lewin. ALE formulation for fluid-structure interaction problems. *Computer methods in applied mechanics and engineering,* 190:659–675, 2000.

[18] B. Van Leer. Towards the ultimate conservative difference scheme. IV. A new approach to numerical convection. *Journal of Computational Physics,* 23:276–299, 1977.

[19] G. Randers-Pehrson and K.A. Bannister. *Airblast loading model for DYNA2D and DYNA3D*. ARL-TR-1310, U.S Army Research Laboratory, Aberdeen Proving Ground, MD, USA, 1997.

[20] L. Schwer. A brief introduction to coupling Load Blast Enhanced with Multi-Material ALE: The best of both worlds for air blast simulation. In *9th LS-DYNA Forum,* pages 1–12, Bamberg, Germany, 2010.

[21] E. L. Lee, H. C. Hornig, and J. W. Kury. *Adiabatic expansion of high explosive detonation products*. TID 4500- UCRL 50422, Lawrence Radiation Laboratory, University of California, CA, USA, 1968.

[22] B. M. Dobratz and P. C. Crawford. *LLNL explosives handbook - properties of chemical explosives and explosive simulants*. UCRL 52997, Lawrence Livermore National Laboratory, University of California, CA, USA, 1985.

[23] J. Wang. *Simulation of landmine explosion using LS-DYNA*. DSTO-TR 1168, Aeronautical and Maritime Research Laboratory, Melbourne, Australia, 2001.

[24] A. Alia and M. Souli. High explosive simulation using multi-material formulations. *Applied Thermal Engineering,* 26(10):1032–1042, July 2006.

[25] D. W. Hyde. *Conventional Weapons Program (ConWep)*. U.S Army Waterways Experimental Station, Vicksburg, MS, USA, 1991.

[26] C. N. Kingery and G. Bulmash. *Airblast parameters from TNT spherical air burst and hemispherical surface burst*. ARBRL-TR-02555, U.S Army BRL, Aberdeen Proving Ground, MD, USA, 1984.

[27] D. Bogosian, J. Ferritto, and Y. Shi. Measuring uncertainty and conservatism in simplified blast models. In *30th Explosives Safety Seminar,* pages 1–26. Atlanta, GA, USA, 2002.

[28] Z. S. Tabatabaei, J. S. Volz, J. Baird, B. P. Gliha, and D. I. Keener. Experimental and numerical analyses of long carbon fiber reinforced concrete panels exposed to blast loading. *International Journal of Impact Engineering,* 57:70–80, 2013.

[29] S. E. Rigby, A. Tyas, T. Bennett, S. D. Clarke, and S. D. Fay. The negative phase of the blast load. *International Journal of Protective Structures,* 5(1):1–20, 2014.

[30] S. A. Granström. *Loading characteristics of air blasts from detonating charges*. Technical Report 100, Transactions of the Royal Institute of Technology, Stockholm, 1956.

[31] N. Aquelet and M. Souli. 2D to 3D ALE mapping. In *10th International LS-DYNA Users Conference,* pages 23–34, Dearborn, MI, USA, 2008.

[32] P. D. Smith, T. A. Rose, and E Saotonglang. Clearing of blast waves from building façades. *Proceedings of the Institution of Civil Engineers - Structures and Buildings,* 134(2):193–199, 1999.

[33] T. A. Rose, P. D. Smith, and J. H. May. The interaction of oblique blast waves with buildings. *Shock Waves,* 16:35– 44, 2006.

[34] G. J. Ballantyne, A. S. Whittaker, G. F. Dargush, and A. J. Aref. Air-blast effects on structural shapes of finite width. *Journal of Structural Engineering,* 136(2):152–159, 2010.